Journal of Power Sources 399 (2018) 443–447

Contents lists available at ScienceDirect

Journal of Power Sources

journal homepage: www.elsevier.com/locate/jpowsour

A combined experimental/theoretical approach to accelerated fuel cell development by quantitative prediction of redox potentials

Kakali Sen[a,b], Andrew Creeth[c,d], Sebastian Metz[b,e,*]

[a] School of Biological Sciences, University of Essex, Wivenhoe Park, Colchester, Essex, CO4 3SQ, UK
[b] Scientific Computing Department, STFC Daresbury Laboratory, Sci-Tech Daresbury, Keckwick Lane, Daresbury, Cheshire, WA4 4AD, UK
[c] ACAL Energy Ltd, The Heath Business and Technical Park, Runcorn, Cheshire, WA7 4QX, UK
[d] AC Chemicals Systems Ltd, c/o Military House, 24 Castle Street, Chester, Cheshire, CH1 2DS, UK
[e] The Hartree Centre, STFC Laboratory, Sci-Tech Daresbury, Keckwick Lane, Daresbury, Cheshire, WA4 4AD, UK

HIGHLIGHTS

- Combined experimental/theoretical method to predict redox potentials of fuel cell catalysts.
- Highly accurate results for broad set of experimental conditions and reference electrodes.
- Simple side chain modifications allow improvement of open circuit voltage of up to 10%.
- Newly identified catalyst with even higher potential providing improvement of ≈25%.

GRAPHICAL ABSTRACT

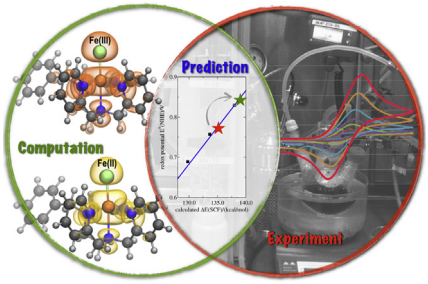

ARTICLE INFO

Keywords:
Redox potential
DFT
Solvent
Reference electrode
Performance optimization

ABSTRACT

This article presents a combined experimental/theoretical approach to accurately predict electrochemical redox potentials based on potential energy calculations. The approach works for experimental setups using different solvents and different reference electrodes and compensates for shortcomings in the prediction of redox potentials originating from the choice of DFT functional, basis set, and solvation model. The methodology is applied to two different sets of iron containing complexes which are used as redox catalysts in Chemically Regenerative Redox Fuel Cells (CRRFCs). For both sets of iron complexes with different 5 N donor ligands, an average deviation to the experimental values of < 0.02V is obtained. Expectedly, the deviation is slightly larger with changes being made in the first coordination shell, but is still within the predictive limit. The scheme is then applied to obtain ligands with both improved properties and lowest production cost.

For the 21st century, fuel cells are regarded as one of the most promising approaches to efficiently convert chemical energy into electrical energy. Conventional Proton Exchange Membrane (PEM) fuel cells use precious metals like platinum to catalyze the oxygen reduction reaction at the cathode:

$$O_2 + 4\,H^+ + 4e^- \rightarrow 2\,H_2O$$

However, catalyst degradation and the cost of high Pt loading prevent the broader commercialization of fuel cells. Recently, very promising results were obtained by use of iron based molecular catalysts [1] in combination with a solution-phase redox mediator by means of a new flow-through cathode [2,3], see Fig. 1. Similar to the approach with molybdenum based polyoxoanions [4,5] the slow oxygen reduction reaction is performed in the bulk solution rather than on the surface of a precious metal electrocatalyst,

* Corresponding author. Scientific Computing Department, STFC Daresbury Laboratory, Sci-Tech Daresbury, Keckwick Lane, Daresbury, Cheshire, WA4 4AD, UK.
E-mail address: Sebastian.metz@stfc.ac.uk (S. Metz).

https://doi.org/10.1016/j.jpowsour.2018.07.056
Received 21 March 2018; Received in revised form 22 June 2018; Accepted 13 July 2018

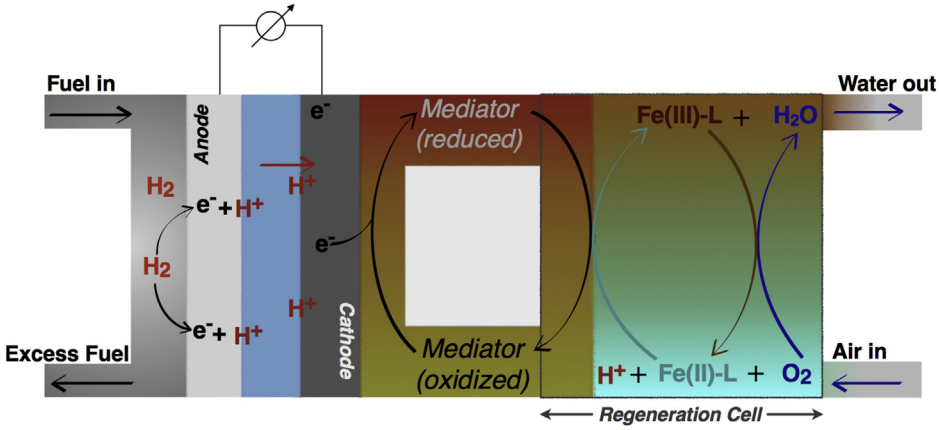

Fig. 1. Schematic working principle of a PEM fuel cell using the FlowCath® technology. Rather than reducing the oxygen at the cathode, an iron complex (Fe(II)L) is used as catalyst to reduce the oxygen with a mediator acting as electron source.

making it very flexible and adaptable when combining different molecular catalysts and mediators [6,7].

A key measurable parameter of catalysts and redox mediators, which relates directly to the voltage efficiency of the redox fuel cell, is the redox potential. Experimentally, the determination of a redox potential itself is a routine measurement, however the synthesis, optimization and purification processes can be very time consuming and costly. A fast, efficient and cheap method to predict accurately the redox potential, especially for smaller modifications of already synthetized complexes would significantly reduce experimental characterization of potential candidates and therefore reduce time to market. It should, however, be kept in mind that a high redox potential and therefore a high cell voltage does not necessarily guarantee a high power fuel cell performance, as this also needs a high current density. The latter, however, does not depend on the redox potential, but on the very complex electron transfer kinetics, which – among others – is influenced by factors like the rate of charge transfer between the cathode and the mediator or the mediator and the iron catalyst in its different intermediate states of oxygen reduction.

Applying computational modelling to predict redox potentials has a surprisingly long history. Already in 1949, Maccoll [8] applied the Hückel theory [9] to establish a correlation between the energies of the lowest unoccupied molecular orbital (LUMO) in conjugated organic molecules and their experimental redox potentials. Since then, more sophisticated quantum mechanical methodologies like density functional theory (DFT) have been applied to predict redox potentials using the Gibbs free energy of a redox couple, ΔG^0, which is directly linked to the standard one-electron redox potential, E^0_{redox}:

$$\Delta G^0 = -FE^0_{redox} \quad (1)$$

The simplest approximation to calculate the change in the Gibbs free energy, ΔG^0, is via frequency calculations of the optimized structures. It can then be obtained from the difference of the potential energy, $\Delta E(SCF)$, and several correction terms (zero point energy correction, $\Delta E(ZPE)$, thermal enthalpy correction, $\Delta H(thermal)$, and thermal entropy correction, $T\Delta S$).

$$\Delta G = \Delta H - T\Delta S = \Delta E(SCF) + \Delta E(ZPE) + \Delta H(thermal) - T\Delta S \quad (2)$$

However, this approximation introduces an unsystematic error and in addition, the frequency calculations, depending on the size of the molecules, can be computationally expensive compared to a normal geometry optimization procedure. On top, the choice of DFT functional, basis set, and solvation model influence the accuracy of the predictions [10–13] leading to too large deviations from the experimental values and therefore preventing an easy use as predictive model. To compensate for these shortcomings, several different computational approaches have been proposed as nicely outlined in the recent review by Truhlar and coworkers [11]. These methods, however, lack the simplicity to be used for screening molecules by non-theoreticians.

To approach the problem at hand with as little resources as possible, we took a combined experimental/theoretical approach: For our predictions, we rely on small, simple and fast potential energy calculations, E (SCF), while substituting the more time consuming calculations by experimental values reported in the literature or from in-house measurements. It is significantly faster than the conventional approaches and therefore affordable for research groups without computational resources beyond a desktop PC e.g. within small and medium sized enterprises (SMEs). In addition, it predicts the redox potentials very accurately with R^2 values of 0.99, see below.

The rationale behind our approach is that for a class of very similar molecules, the correction terms in equation (2) are considered to be approximately constant, resulting in a correlation between the redox potential, E^0_{redox}, and the corresponding potential energy, $\Delta E(SCF)$:

$$E^0_{redox} \sim \Delta E(SCF) + const \quad (3)$$

In order to obtain the redox potentials relative to the normal hydrogen electrode $E^0(NHE)$, (or any other reference electrode) the values for the hydrogen half-reaction can also be included in the constant providing a correlation between the standard electrode potentials relative to the normal hydrogen electrode, $E^0(NHE)$, and the energy difference between two redox states of the investigated molecule, in our case between the Fe(II) and the Fe(III) states of the iron complexes:

$$E^0(NHE) \sim E(SCF,\ Fe(II)L) - E(SCF,\ Fe(III)L) + const \quad (4)$$

Of particular interest for this study were iron complexes with 5 N donor ligands based on the trilen and the N4Py structures (Scheme 1). The starting geometries of the three complexes [Fe(II)trilen (R = H/Cl/SO_3Na)-OH_2]$^{2+}$ were obtained by manually substituting the functional groups of the ligand and exchanging Cl^- to H_2O in the crystal structure of [Fe(II)trilen (R = H)-Cl]$^+$ [14]. The same procedure was followed to generate the starting geometry of [Fe(II)N4Py(R = H/CH_3)-OH_2]$^{2+}$ from the crystal structure of [Fe(II)N4Py(R = H)-Cl]$^+$ [15]. Crystal structures for [Fe(II) (Bz-tpen)-X] with X = CH_3COO^-/OCN^-/Cl^-/SCN^-/Br^-/I^-/CH_3CN [16–18] and [Fe(III) (Bz-tpen)-X] with X = CH_3O^- [19], [20] were directly taken from the literature and were modified manually to obtain starting geometries for X = OH^-/F^-.

The initial structures were optimized using the B3LYP hybrid functional [21–26], which has been used for redox calculations [10,12,27,28]. The B3LYP functional is also known to correctly predict the lowest energy spin state of iron complexes [28,29] (see also supporting information for details), in combination with the def2-SVP basis set [30], which has also demonstrated to provide good geometries for transition metal complexes [31–33]. All calculations were performed using the ORCA software package [34]. Single point calculations were performed on top of the optimized geometries using the def2-TZVP basis set [30,35] together with the COSMO methodology [36] (using ε = 36.6 for acetonitrile and ε = 80.4 for water as solvent).

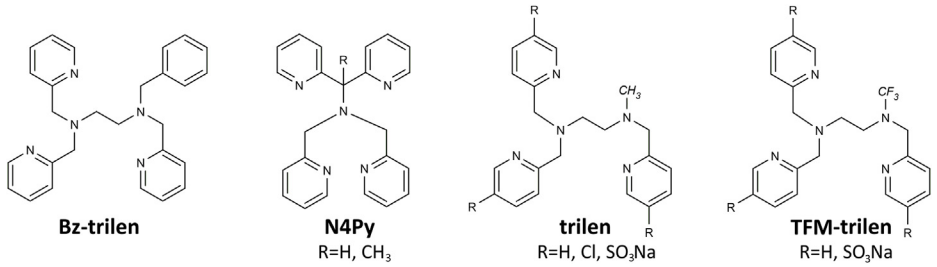

Scheme 1. Structure of the three used 5-N donor ligands used for parametrization and the fluorinated trilen ligand containing the trifluoromethyl (TFM) group.

1. Iron complexes with the same 5N-ligand: Bz-trilen complexes in acetonitrile

Our first set of structures is based on iron complexes with the same Bz-trilen ligands, see Scheme 1. For all structures, three spin states were calculated for both Fe(II) and Fe(III) species: Singlet, triplet and quintet for the Fe (II) state and doublet, quartet and sextet for the Fe(III) state (for details see SI). All Fe(II) complexes converged to a high spin (quintet) as their ground state, except from [Fe(II) (Bz-tpen)-$NCCH_3$]$^{2+}$, for which the ground state is a singlet, in agreement with experimental findings [17]. All Fe(III) complexes have a sextet as lowest spin state, except from [Fe(III) (Bz-tpen)-$NCCH_3$]$^{3+}$ and [Fe(III) (Bz-tpen)-OH]$^{2+}$, for which the ground state is a doublet. For Fe (Bz-tpen)-$NCCH_3$, this demonstrates the influence of the π^* orbitals of the $NCCH_3$ molecule, which interact with the d-orbitals of the iron, therefore stabilizing a low spin configuration in both oxidation states. The energy difference between the lowest energy state of the Fe(II) and the Fe(III) species, ΔE (SCF), is plotted against the experimental redox potential, in this case E^0(Fc/Fc$^+$), see Fig. 2.

It is evident, that due to the combination of experimental and theoretical values, the predicted values for E^0(Fc/Fc$^+$) are highly accurate (R^2 = 0.99), see Table 1. Therefore the methodology can be used to quantify the effect of changes in the first coordination shell of the redox active complexes. This holds equally true for different spin states, as demonstrated for the Fe(Bz-tpen)-$NCCH_3$ complex.

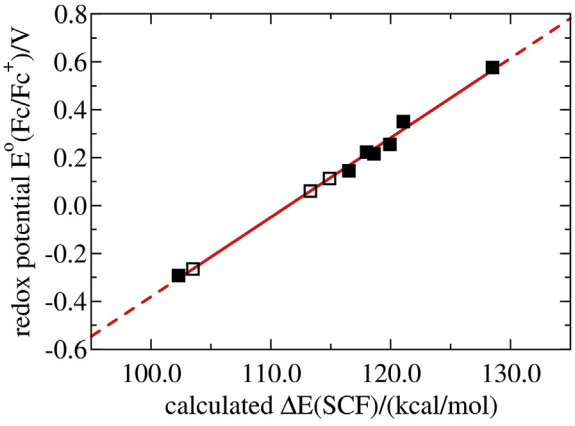

Fig. 2. Correlation between the calculated energy difference between the Fe(II) and Fe(III) structures, ΔE (SCF) and the redox potential E^0(Fc/Fc$^+$). The filled squares are the values obtained from the experimental redox potentials for [Fe (II) (Bz-tpen)-X] with X = CH_3O^-/OCN^-/Cl^-/SCN^-/Br^-/I^-/CH3CN coordinating to the iron center. The open squares show the calculated values for X = OH^-/F^-/CH_3COO^-. The dashed lines demonstrate the extrapolation beyond the measured range of redox potentials. For details see also Table 1.

The calculated set of structures all have 5 N ligand donors, straightforwardly justifying that the thermal and entropic corrections can be approximated as constant, see equation (3). The important task remains to validate whether the methodology works for a different solvent/reference electrode and, more importantly for changes in the ligand. The following section demonstrates complexes with modified ligands in water.

2. Ligand modifications: aqueous trilen and N4Py complexes

Our second set of structures is based on iron complexes with different 5 N donor ligands related to trilen and N4Py, see Scheme 1. As in the previous case, for all structures, three spin states were calculated for both Fe(II) and Fe(III) states; singlet, triplet and quintet for the Fe(II) state and doublet, quartet and sextet for the Fe(III) state (for details see SI). All Fe(II) complexes converged to a high spin (quintet) as their ground state, except from Fe(II)N4Py(R = Me), for which the ground state is a singlet. While the energy difference is very small, this is in agreement with significant changes observed in the UV/vis spectrum of Fe(II)N4Py(R = H) and Fe(II)N4Py(R = Me). The lowest spin state of all Fe(III) complexes is a doublet. The energy difference between the lowest energy state of the Fe(II) and the Fe(III) species, ΔE (SCF), is plotted against the experimental redox potential, in this case E^0(NHE), see Fig. 3.

As for the previous case, due to the combination of experimental and theoretical values, the predicted values for E^0(NHE) are highly accurate (R^2 = 0.99), see Table 2. The methodology then can be used to quantify the effect of adding electron donating (R = CH_3) and electron withdrawing (R = CF_3,CN) groups to the ligand. The electron withdrawing groups reduce the electron density of the ligand in the vicinity of the iron center and therefore reduce the stabilization by coulombic interactions between the ligand and the iron center. This effect is stronger for the higher charged Fe(III) than for the Fe(II) center and the energy gap between the two species increases, resulting in a higher redox potential. Depending on the substituents, R, different ligands might cause a change of the pH in solution, which will influence the redox potential. For the measurements of the redox potentials it is

Table 1
Calculated energy difference between the Fe(II) and Fe(III) structures, ΔE (SCF), and the resulting redox potential E^0(Fc/Fc$^+$) in acetonitrile for Fe(Bz-tpen)-X. The experimental values are given in parenthesis.

X	CH_3O^-	OH^-	F^-	CH_3COO^-	OCN^-	Cl^-	SCN^-	Br^-	I^-	CH_3CN
ΔE (SCF)/(kcal/mol)	102.3	103.5	113.3	114.9	116.5	118.6	118.0	119.9	112.1	128.5
E^0(Fc/Fc$^+$)/V	−0.305 (−0.293[a])	−0.265	0.060	0.113	0.167 (0.145[b])	0.237 (0.216[b])	0.216 (0.223[b])	0.281 (0.255[b])	0.318 (0.350[b])	0.565 (0.576[b])

[a] Averaged value for RO^- taken from Table 2 of Flores-Leonar [37].
[b] Taken from Ortega-Villar [17].

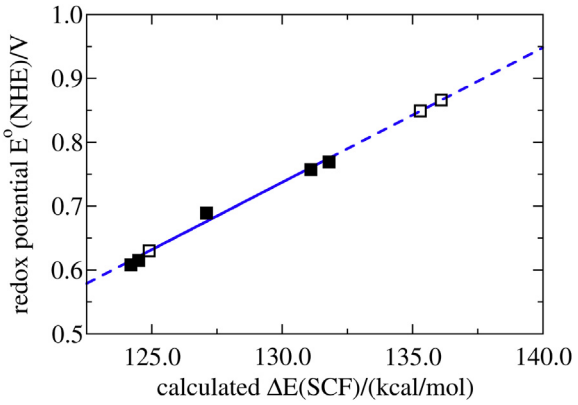

Fig. 3. Correlation between the calculated energy difference between the Fe(II) and Fe(III) structures, ΔE (SCF) and the redox potential E^0(NHE). The filled squares are the values obtained from the experimental complexes [Fe(II)trilen (R = H/Cl/SO_3Na)-OH_2]$^{2+}$ and [Fe(II)N4Py(R = H/CH_3)-OH_2]$^{2+}$. The open squares show the calculated values for the complexes [Fe(II)trilen (R = CH_3/CF_3/CN)-OH_2]$^{2+}$. The dashed lines demonstrate the extrapolation beyond the measured range of redox potentials. For details see also Table 2.

important to ensure that they are carried out under the same experimental conditions.

Predicting the redox potential of unknown ligands may involve extrapolation beyond the known experimental range (0.608V–0.780V, solid line in Fig. 3), as by default we try to identify complexes with higher redox potentials than the ones already measured experimentally. The improvement in open circuit voltage for the best candidate (R = CN) is ≈ 10%.

3. Fine tuning of ligand properties: aqueous TFM-trilen complexes

Results from the previous section suggest that trilen (R = CN) should be used as new experimental lead structure. However, replacing the SO_3Na group reduces the solubility of the complexes and adding a reactive CN group can cause side reactions and degradation of the catalyst. The trifluoromethyl (TFM) group exerts a similar electron withdrawing effect as CN, but is chemically inert. By changing the trilen ligand into TFM-trilen, see Scheme 1, we are able to increase the redox potential by roughly 0.2V, see Table 3. TFM-trilen (R = SO_3Na) with a predicted redox potential of 0.976V proves to be the best ligand among the series studied by allowing for an increased open circuit voltage of ≈25%, reducing side reactions of the active oxygen species with the methyl group of the trilen ligand and maintaining its solubility. A potential synthetic route for the predicted ligand is outlined in Scheme 2, using H-trilen as synthetized by Mialane et al. [38] and then converting its N-H group into a N-CF_3 group [39,40]. Having identified a catalyst with significantly increased redox potential, the future progress depends on the synthesis of improved ligands and the identification of improved mediator molecules which match the redox properties of the new catalysts, while maintaining a high current density.

Table 3
Calculated energy difference between the Fe(II) and Fe(III) structures, ΔE (SCF), and the predicted redox potential E^0(NHE) for equivalent trilen and TFM-trilen complexes. It should be noted that a high redox potential on its own does not guarantee a high performance fuel cell.

	trilen (R = H)	trilen (R = SO_3Na)	TFM-trilen (R = H)	TFM-trilen (R = SO_3Na)
ΔE (SCF)/(kcal/mol)	127.1	131.8	136.4	141.3
E^0(NHE)/V	0.676	0.775	0.872	0.976

4. Conclusion

The combined experimental/theoretical method as described and validated above provides an elegant way of calculating highly accurate redox potentials in different solvents and with different reference electrodes while requiring only a limited number of parameters: a starting geometry (generally based on crystal structures of similar molecules) and a limited amount of redox potentials, measured under the same experimental conditions. No *a priory* information about the spin states of the metal center is needed. This method provides a simple, cheap and efficient way to guide and direct development of a class of similar molecules having a direct impact on the performance of redox fuel cells.

In the actual case of iron catalysts, as analyzed by the above method, the redox potential increases with addition of electron withdrawing groups (R = CN/CF_3/SO_3Na) and decreases with electron donating groups (R = CH_3). The key parameter influencing the redox potential is the amount of electron density at the donor atoms of the ligand coordinating to the iron center. This effect is stronger for the higher charged Fe(III) than for the Fe(II) center and the energy gap between the two species increases, resulting in a higher redox potential. This effect is stronger the closer the electron withdrawing group is located to redox active center, as evident from the TFM-trilen case.

Table 2
Calculated energy difference between the Fe(II) and Fe(III) structures, ΔE (SCF), and the predicted redox potential E^0(NHE) for different 5 N donor ligands in aqueous solution. The experimental values are given in parenthesis. It should be noted that a high redox potential on its own does not guarantee a high performance fuel cell.

	N4Py (R = H)	N4Py (R = CH_3)	trilen (R = CH_3)	trilen (R = H)	trilen (R = Cl)	trilen (R = SO_3Na)	trilen (R = CF_3)	trilen (R = CN)
ΔE (SCF)/(kcal/mol)	124.2	124.5	124.9	127.1	131.1	131.8	135.3	136.1
E^0(NHE)/V	0.615 (0.608[a])	0.621 (0.615[a])	0.630	0.676 (0.689[a])	0.761 (0.757[a])	0.775 (0.780[b])	0.849	0.866

[a] Taken from Ref. [7].
[b] This work.

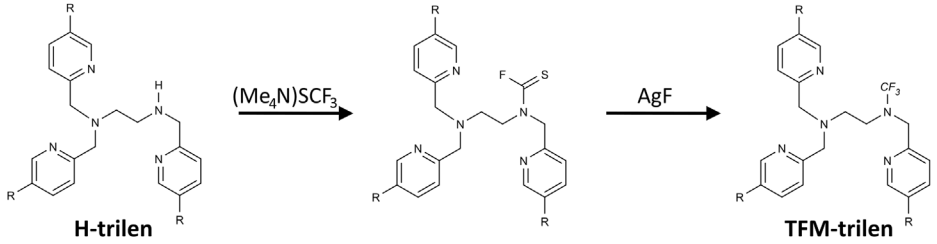

Scheme 2. Synthetic route for conversion of H-trilen intoTFM-trilen.

Notes

The authors declare no competing financial interests.

Acknowledgment

The authors would like to thank David Rochester (now Lancaster University) and Kathryn Knuckey (now University of Liverpool) for the fruitful discussions and for sharing their expertise and insights. We would like to thank Dr. Thomas Smith for the permission to use his pictures in the TOC graphic. SM was supported by EPSRC grant EP/N510038/1. We acknowledge the computing resources provided by STFC Scientific Computing Department's SCARF cluster and the use of Hartree Centre resources in this work. The STFC Hartree Centre is a research collaboratory in association with IBM providing High Performance Computing platforms funded by the UK's investment in e-Infrastructure.

Appendix A. Supplementary data

Supplementary data related to this article can be found at https://doi.org/10.1016/j.jpowsour.2018.07.056.

References

[1] F. Jaouen, E. Proietti, M. Lefèvre, R. Chenitz, J.-P. Dodelet, G. Wu, H.T. Chung, C.M. Johnston, P. Zelenay, Energy Environ. Sci. 4 (2011) 114–130.
[2] R. Singh, A. Shah, A. Potter, B. Clarkson, A. Creeth, C. Downs, F. Walsh, J. Power Sources 201 (2012) 159–163.
[3] Y.V. Tolmachev, M.A. Vorotyntsev, Russ. J. Electrochem. 50 (2014) 403–411.
[4] N.L. Gunn, D.B. Ward, C. Menelaou, M.A. Herbert, T.J. Davies, J. Power Sources 348 (2017) 107–117.
[5] D.B. Ward, N.L. Gunn, N. Uwigena, T.J. Davies, J. Power Sources 375 (2018) 68–76.
[6] K. Knuckey, D. Rochester and A. Creeth, Acal Energy Ltd, Redox Fuel Cells, US patent 8647781 B2, United States, 2014.
[7] K. Knuckey and A. Creeth, Acal Energy Ltd, Fuel Cells, US patent 9136554 B2, United States, 2015.
[8] A. Maccoll, Nature 163 (1949) 178.
[9] E. Hückel, Z. Phys. 70 (1931) 204–286.
[10] S.J. Konezny, M.D. Doherty, O.R. Luca, R.H. Crabtree, G.L. Soloveichik, V.S. Batista, J. Phys. Chem. C 116 (2012) 6349–6356.
[11] A.V. Marenich, J. Ho, M.L. Coote, C.J. Cramer, D.G. Truhlar, Phys. Chem. Chem. Phys. 16 (2014) 15068–15106.
[12] T.F. Hughes, R.A. Friesner, J. Chem. Theor. Comput. 8 (2012) 442–459.
[13] J.J. Guerard, J.S. Arey, J. Chem. Theor. Comput. 9 (2013) 5046–5058.
[14] I. Bernal, I.M. Jensen, K.B. Jensen, C.J. McKenzie, H. Toftlund, J.-P. Tuchagues, J. Chem. Soc., Dalton Trans. (1995) 3667–3675.
[15] G. Roelfes, M. Lubben, K. Chen, R.Y. Ho, A. Meetsma, S. Genseberger, R.M. Hermant, R. Hage, S.K. Mandal, V.G. Young Jr., Inorg. Chem. 38 (1999) 1929–1936.
[16] A. Hazell, C.J. McKenzie, L.P. Nielsen, S. Schindler, M. Weitzer, J. Chem. Soc., Dalton Trans. (2002) 310–317.
[17] N. Ortega-Villar, V.M. Ugalde-Saldívar, M.C. Muñoz, L.A. Ortiz-Frade, J.G. Alvarado-Rodríguez, J.A. Real, R. Moreno-Esparza, Inorg. Chem. 46 (2007) 7285–7293.
[18] T. Nebe, A. Beitat, C. Würtele, C. Dücker-Benfer, R. van Eldik, C.J. McKenzie, S. Schindler, Dalton Trans. 39 (2010) 7768–7773.
[19] N. Ortega-Villar, M.C. Muñoz, J.A. Real, Eur. J. Inorg. Chem. 2010 (2010) 5563–5567.
[20] N. Ortega-Villar, A.Y. Guerrero-Estrada, L. Piñeiro-López, M.C. Muñoz, M. Flores-Álamo, R. Moreno-Esparza, J.A. Real, V.M. Ugalde-Saldívar, Inorg. Chem. 54 (2015) 3413–3421.
[21] J.C. Slater, Phys. Rev. 81 (1951) 385–390.
[22] S.H. Vosko, L. Wilk, M. Nusair, Can. J. Phys. 58 (1980) 1200–1211.
[23] A.D. Becke, Phys. Rev. 38 (1988) 3098–3100.
[24] A.D. Becke, J. Chem. Phys. 98 (1993) 1372–1377.
[25] P.J. Stephens, F.J. Devlin, C.F. Chabalowski, M.J. Frisch, J. Phys. Chem. 98 (1994) 11623–11627.
[26] C. Lee, W. Yang, R.G. Parr, Phys. Rev. B 37 (1988) 785–789.
[27] L.E. Roy, E. Jakubikova, M.G. Guthrie, E.R. Batista, J. Phys. Chem. 113 (2009) 6745–6750.
[28] H. Kim, J. Park, Y.S. Lee, J. Comput. Chem. 34 (2013) 2233–2241.
[29] M. Swart, A.R. Groenhof, A.W. Ehlers, K. Lammertsma, J. Phys. Chem. 108 (2004) 5479–5483.
[30] A. Schäfer, H. Horn, R. Ahlrichs, J. Chem. Phys. 97 (1992) 2571–2577.
[31] G. Dong, S. Shaik, W. Lai, Chem. Sci. 4 (2013) 3624–3635.
[32] S. Roy, J. Kästner, Angew. Chem. Int. Ed. 55 (2016) 1168–1172.
[33] S. Metz, Inorg. Chem. 56 (2017) 3820–3833.
[34] F. Neese, WIREs Comput. Mol. Sci. 2 (2012) 73–78.
[35] F. Weigend, R. Ahlrichs, Phys. Chem. Chem. Phys. 7 (2005) 3297–3305.
[36] A. Klamt, G. Schüürmann, J. Chem. Soc., Perkin Trans. 2 (5) (1993) 799–805.
[37] M.M. Flores-Leonar, R. Moreno-Esparza, V.M. Ugalde-Saldívar, C. Amador-Bedolla, ChemistrySelect 2 (2017) 4717–4724.
[38] P. Mialane, A. Nivorojkine, G. Pratviel, L. Azema, M. Slany, F. Godde, A. Simaan, F. Banse, T. Kargar-Grisel, G. Bouchoux, Inorg. Chem. 38 (1999) 1085–1092.
[39] T. Milcent, B. Crousse, Compt. Rendus Chem. 21 (8) (2018) 771–781.
[40] T. Scattolin, K. Deckers, F. Schoenebeck, Angew. Chem. 129 (2017) 227–230.